Nuclear Instruments and Methods in Physics Research A 638 (2011) 24–32

Contents lists available at ScienceDirect

Nuclear Instruments and Methods in Physics Research A

journal homepage: www.elsevier.com/locate/nima

Intrinsic resolutions of DEPFET detector prototypes measured at beam tests

L. Andricek [a], J. Caride [b], Z. Doležal [c], Z. Drásal [c], S. Esch [d], A. Frey [e], J. Furletova [d], S. Furletov [d], C. Geisler [e], S. Heindl [f], C. Iglesias [b], J. Knopf [g], M. Koch [d], P. Kodyš [c,*], C. Koffmane [a,h], C. Kreidl [g], H. Krüger [d], P. Kvasnička [c], C. Lacasta [i], L. Malina [c], C. Mariñas [i], J. Ninkovic [a], L. Reuen [d], R.H. Richter [a], S. Rummel [a], J. Scheirich [c], J. Schneider [d], B. Schwenker [e], P. Vázquez [b], M. Vos [i], T. Weiler [f], N. Wermes [d]

[a] Max-Planck-Institut für Physik and MPI Halbleiterlabor, München, Germany
[b] Facultade de Fisica, Universidade de Santiago de Compostela, Santiago de Compostela, Spain
[c] Faculty of Mathematics and Physics, Institute of Particle and Nuclear Physics, Charles University, V Holešovičkách 2, 18000 Prague, Czech Republic
[d] Physikalisches Institut, Universität Bonn, Bonn, Germany
[e] II. Physikalisches Institut, Universität Göttingen, Göttingen, Germany
[f] Institut für Experimentelle Kernphysik, Karlsruher Institut für Technologie, Karlsruhe, Germany
[g] Institut für Technische Informatik, Universität Heidelberg, Mannheim, Germany
[h] Fakultät Elektrotechnik und Informatik, Technische Universität Berlin, Berlin, Germany
[i] Instituto de Física Corpuscular, IFIC/CSIC-UVEG, Valencia, Spain

ARTICLE INFO

Article history:
Received 12 November 2010
Received in revised form
16 January 2011
Accepted 1 February 2011
Available online 22 February 2011

Keywords:
Silicon pixel detector
Detector resolution
Spatial resolution
DEPFET
Beam test

ABSTRACT

The paper is based on the data of the 2009 DEPFET beam test at CERN SPS. The beam test used beams of pions and electrons with energies between 40 and 120 GeV, and the sensors tested were prototypes with thickness of 450 μm and pixel pitch between 20 and 32 μm. Intrinsic resolutions of the detectors are calculated by disentangling the contributions of measurement errors and multiple scattering in tracking residuals. Properties of the intrinsic resolution estimates and factors that influence them are discussed. For the DEPFET detectors in the beam test, the calculation yields intrinsic resolutions of ≈ 1 μm, with a typical accuracy of 0.1 μm. Bias scan, angle scan, and energy scan are used as example studies to show that the intrinsic resolutions are a useful tool in studies of detector properties. With sufficiently precise telescopes, detailed resolution maps can be constructed and used to study and optimize detector performance.

1. Introduction

Experiments in future colliders like the ILC or the super B factories require excellent vertexing performance. The requirements on state-of-the-art vertex detectors for high-energy physics experiments combine excellent vertex reconstruction, achievable only by a highly granular pixel detector, with fast readout and minimum material budget to reduce the impact of multiple Coulomb scattering on the measurement. This severely constrains sensor thickness, power consumption, and design of detector services.

The DEPFET collaboration pursues the development of vertex detectors based on the concept of the depleted field effect transistor. The concept (see Fig. 1) originated in 1987 and has been published in Refs. [1–4]. Briefly, each DEPFET pixel has an integrated p-MOS transistor. Sideward depletion creates a potential minimum for electrons in the internal gate under the channel. Electrons collected in the internal gate modulate the transistor current. They can be removed from the internal gate via a clear contact.

The present paper contains beam test results with special focus on intrinsic resolution of DEPFET detectors. The intrinsic resolution of a detector is defined as the root-mean-square error of position measurement in the detector. The reason for a separate paper on intrinsic resolutions is their importance not only *per se* as a measure of accuracy of the positional information provided by the detector, but also as a versatile tool for studies of various detector properties (such as detector depletion voltage and charge sharing) and analysis procedures (such as hit reconstruction or alignment).

Systematic studies of DEPFET spatial resolutions started in 2006 [5], and continued in the following years [6].

Estimation of intrinsic resolutions is a relatively straightforward procedure, though somewhat numerically subtle; the task is to decompose the tracking residuals to contributions of multiple scattering and measurement errors, based on known statistics of both.

A fairly extensive description of beam test data analysis is presented with a view to show how individual steps of the analysis, such as hit reconstruction, alignment and tracking, mechanical instabilities, and irregularities in detector response, influence intrinsic detector resolutions. Results of a Monte Carlo simulation study illustrate the consistency of resolution estimates.

* Corresponding author. Tel.: +420737665620; fax: +420221912434.
E-mail address: peter.kodys@mff.cuni.cz (P. Kodyš).

0168-9002/$ - see front matter © 2011 Published by Elsevier B.V.
doi:10.1016/j.nima.2011.02.015

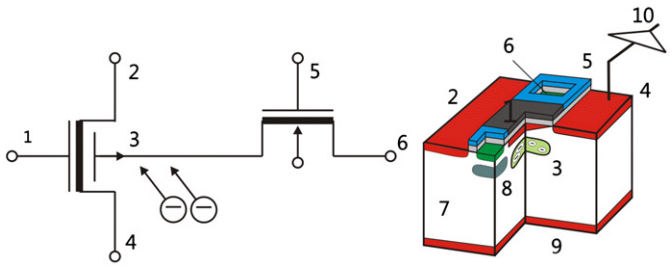

Fig. 1. The principle of DEPFET. 1—external FET gate, 2—p^+ source, 3—deep n-doped internal gate, 4—p^+ drain with connection to external amplifier, 5—clear gate, 6—n^+ clear, 7—depleted n-Si bulk, 8—deep p-well, 9—p^+ backside contact, 10—amplifier.

The usefulness of detector resolutions is illustrated by showing the results of beam energy scan, bias scan and angle scan in terms of detector resolutions. Detailed results on the variation of detector resolutions within the area of a detector pixel illustrate another useful application.

2. DEPFET beam test

The beam test setup was built of six detectors as close to one another as allowed by the position stages to minimize the effects of multiple scattering. Particles were triggered by two scintillators in front of and behind the setup.

Five matrices of the same type were used as reference planes. Their parameters were kept constant during beam test experiments. The Devices Under Tests (DUTs) were three structures designed specially for the ILC conditions, with small pixels and high spatial resolution. The thickness of all matrices was 450 μm. Matrices with 64×256 pixels, pixel pitch 20×20, 24×24 or 32×24 μm were used.

The geometry of the 2009 beam test is shown in Fig. 2. The DUT was placed in position 2.

Fig. 3 shows the orientation of the (local) detector coordinate system relative to the layout of chips on a DEPFET hybrid.

The six detectors of the setup were synchronized with a EUDET Trigger Logic Unit [7] and operated from a Linux workstation.

Tracks passing through all six detectors were found in about 25% events, the inefficiency being mainly due to triggering by a $2.4 \times 6.5\ \mathrm{mm}^2$ scintillator at the front of the setup. A typical acquisition rate with 120 GeV pion beam was in the order of 1000 events per minute (uncorrected for the spill structure of the SPS).

The basic set of beam test studies consists of

a bias scan from 100 to 200 V,

an angle scan of $-6/+4^\circ$ tilt of the DUT around horizontal axis,[1] and

an energy scan for beam energies from 40 to 120 GeV, comprising separate runs with electron beams (40, 60, 80, and 100 GeV) and pion beams (80, 100, and 120 GeV).

3. Specific properties of DEPFET detectors

DEPFET detectors have some special features that have to be explained in order to understand the beam test analysis and its results.

[1] The angle scan was actually performed at the 2008 DEPFET beam test that took place at the same site and with similar setup.

3.1. Noise and intrinsic resolution

In DEPFET detectors, noise is dominated by the front-end electronics and was about $\sqrt{\langle i^2 \rangle} \approx 120$ nA for all detectors, where a typical amplification in pixel is about 0.5 nA/e^-. Response to 120 GeV pions (110 keV deposited energy) was over 14.6 μA for the large pixel pitch (signal to noise ratio about 120), and 25.3 μA for the small pixel pitch (signal to noise ratio 200) [8]. In combination with fine pitch, the high *S/N* ratios result in intrinsic resolutions between 1 and 2 μm (see the Results section below). With these parameters, multiple scattering effects are very important at the nominal beam energy of the beam test, 120 GeV, and become dominant at the lower beam energies (down to 40 GeV) used in the energy scan.

3.2. Pixel structure

The elementary cell of a DEPFET matrix comprises 1×2 pixels as shown in Fig. 7; indeed, for the fine coordinate (*y*, the dimension with 256 pixels) a pattern with 2-pixel period can be identified in the sensor design, see Fig. 4. The "large ILC" pixel design (Fig. 4, right) was used in the reference planes, and the "smallest ILC" and "small ILC" pixel designs (Fig. 4 left and center) were used for the DUTs (module 2). The data analysis has to respect this specific feature, for example, in the calculation of η corrections.

3.3. Edge effect and other positional response distortions

The edge effect is a systematic shift of charge generated by particles in the detector bulk towards the perimeter of the detector's active area. It has been observed in all DEPFET beam tests as a systematic bias in the positional information reported by the detectors. Later it was confirmed by laser tests (Fig. 5). The distortion affects a zone of up to 250 μm around the perimeter of a detector's active area. The effect arises from a potential difference between the interior of the detector's active area and the outer ring, the latter potential being higher by about +10 V. An appropriate setting of the outer ring voltage can suppress the effect. Other types of response distortions have been observed in previous beam tests. They include *V-effects* (shift between the two halves of a sensor) and periodic distortions. They are less pronounced and are corrected in the same way as edge effects. By careful configuration of detector settings, they were strongly suppressed in the 2009 beam test.

4. Data analysis

Beam test data were analyzed by three groups using different approaches and software tools. The results were cross-checked up to the level of tracking residuals and all discrepancies between the results of the three groups have been thoroughly investigated and are currently well understood. The results presented in this paper are based on consensual estimates of the three analyses.

4.1. Data analysis chain

The data analysis chain comprises the following steps:

Raw data inspection and frame display: check consistency and arrangement of data; identify exposed regions on detectors; mask channels with wrong response.

Black correction: estimate pedestals and common mode noise (CMN) as medians of signals; subtract pedestals and CMN from frame data; estimate RMS channel noises as median absolute deviations of channel signals.

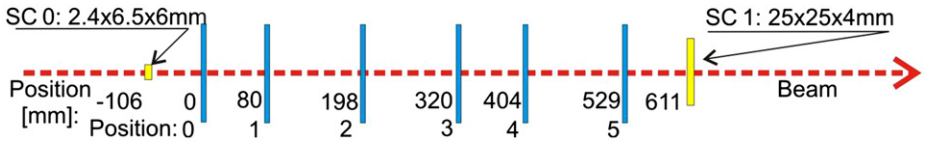

Fig. 2. Arrangement of sensors in the 2009 beam test.

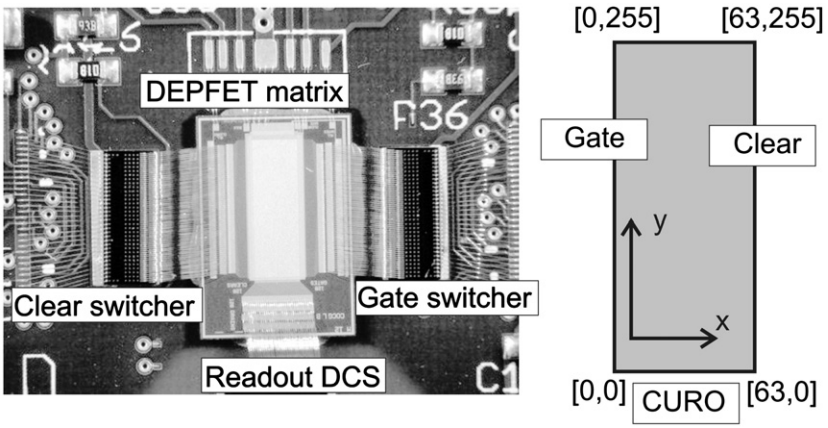

Fig. 3. Layout of chips on a hybrid (left) and the detector coordinate system (right).

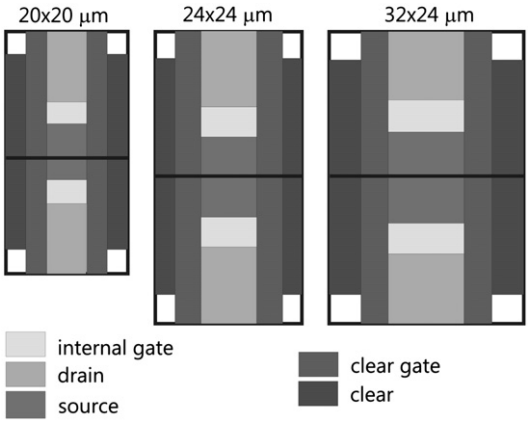

Fig. 4. The design of a 1×2 pixels area for the smallest (left), small (center) and large (right) ILC pixel design.

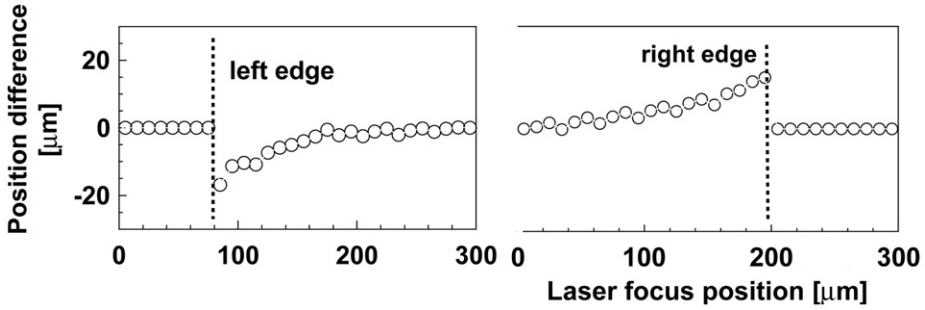

Fig. 5. Edge effect as seen in a laser scan study. The mean difference between the reconstructed position (without η correction) of exposure and actual position of the laser focus is shown as a function of the focus position. The width of laser beam at its waist was about 3 μm. Intensity of the 682 nm laser was attenuated to produce approximately the charge of a MIP per pulse. Each circle is a mean of 1000 measurements. See Ref. [6] for details of the laser scanning setup.

White correction: estimate pixel gains using maximum-likelihood equalization of seed distributions; pixel gains are applied in hit reconstruction when a reliable value different from 1 is available.

Hit reconstruction: identify signal clusters; estimate hit positions using center of gravity and η correction (see below in the list) based on groups of 2×2 (large pixel size) or 3×3 (small pixel size) signals around the highest signal of a cluster.

Track formation: combine hits on various detectors into particle tracks using the Scott and Longuet-Higgins [9] similarity matrix deconvolution. Only tracks with exactly one hit in every sensor (and hits belonging to such tracks) are used in the following analysis.

η corrections are calculated using only hits that belong to tracks; two one-dimensional η corrections [10] are calculated for the x and y projections of 2×2 pixels' area for each sensor.

Track fitting and sensor alignment: parameterize particle tracks; estimate intersections of tracks with detectors; correct for detector misalignment. A cut of 250 μm around the perimeter of each detector was used to eliminate edge effects.

Correction for mechanical movements: regularly update alignment to account for slow mechanical drifts in detector positions (typical time scale tens of minutes). See Section 5.2 for more details.

Correction of response distortions: use patterns in tracking residuals to correct for systematic bias of the detector's positional response. See Section 5.3 for more details.

Calculation of detector resolutions: estimate detector resolutions, tracking errors, telescope pointing resolution at DUT plane, etc. See Section 5.1 for more details.

4.2. Analysis software

For analysis, the ILCSoft/EUTelescope [11] analysis package with special extensions for DEPFET sensors [12] was used by two groups, while the third group used their own ROOT-based [13] analysis package allowing also intrinsic resolution calculations.

5. Notes on selected analysis methods

This section gives some more detail on selected steps of the analysis. The level of detail for individual steps was chosen in correspondence with the focus of the paper.

5.1. Calculation of detector resolutions

Detector resolution is the RMS error of the position measurement in the detector. The resolutions are calculated from the covariance matrix of track fit residuals. Each fit residual is a linear combination of detector measurement errors and multiple scattering deflections. Therefore, residual covariance is a linear combination of measurement error covariance and multiple scattering covariance:

$$cov(\hat{u}^c) \equiv \langle (u^c-\hat{u}^c)(u^c-\hat{u}^c)^T \rangle = H(G\Sigma^2 G^T+\Delta^2)H \quad (1)$$

where u^c are the local hit coordinates and $\hat{u}^c$ are the local coordinates of track intersection with sensor plane, H is the projector to the residual space. If the track is fitted with a line, $u=F\beta$, with F the factor matrix and β the vector of line intercepts and slopes, then $H=I-F(F^{TF})^{-1}F^T$, G describes the geometry of multiple scattering. In the simplest case, $G_{ij}=(z_j-z_i)_+$ with z_i being the z coordinate of the i-th detector, Σ is the diagonal matrix with squared RMS multiple scattering deflections on the diagonal, Δ is the diagonal matrix with squared detector resolutions on the diagonal.

The RMS multiple scattering deflections in Σ can be calculated using the Moliére formula [16], so detector resolutions in Δ can be expressed in terms of (experimental) residual correlations and (theoretical) RMS multiple scattering deflections.

Formally, resolutions can be calculated by solving Eq. (1) for Δ. The procedure is complicated by the fact that H does not have full rank: its rank is $2\times$(number of points on the track)-4. Using matrix algebra, the resolutions can be expressed in terms of pseudoinverses of $H\circ H$, which is equivalent to a least-squares fit to the diagonal of the covariance matrix.

Another, more straightforward method is to find the resolutions by a maximum-likelihood fit to the data using a non-linear fitter. Such estimate uses the full covariance matrix, but gives very similar estimates as the "diagonal" estimator described above. It is significantly more stable than the "diagonal" estimator in the large multiple scattering regime, but in that regime both estimators behave very poorly.

A strong test of the quality of intrinsic resolution estimates is by varying the detector setup. If data from a selected module are omitted from the analysis (keeping the module in the setup, however, as passive material and a source of multiple scattering), the resolutions on the remaining detectors have to stay the same as with the "full" setup—except, possibly, a larger statistical error. However, small systematic, geometry-dependent deviations are observed in these calculations. They are apparently related to poor numerical properties of the problem, in particular, to (effective) inversion of an ill-conditioned matrix $H\circ H$. For the beam test data shown in this paper, a typical systematic error was 0.1 μm in both coordinates.

The key test of resolution estimates is beam energy scan. It allows to use the traditional method of resolution calculation by extrapolation to zero multiple scattering, the so-called "infinite energy extrapolation". The method is based on the observation that the only beam energy dependent term in Eq. (1) is $H(G\Sigma^2G^T)H$, and this term vanishes as $E\to\infty$. Indeed, by Moliére's formula [16], $\Sigma\sim 1/p$, and $E\sim pc$ for relativistic particles. Thus, plotting mean squared residuals in the DUT plane vs. $1/E^2$ gives a straight line with intercept equal to the sum of squared DUT resolution plus squared telescope system resolution in the DUT plane. If telescope resolutions are known, then DUT resolution can be calculated.

Since this is a "cleaner" method as it does not rely on a specific model of multiple scattering, it is a good reference for the quality assessment of resolution estimators. Unfortunately, we have repeatedly found that a practical realization of the energy scan with a sufficiently broad range of beam energies at CERN's SPS is by itself a difficult task, as will be discussed later in the corresponding results section.

5.2. Mechanical stability

Mechanical instabilities degrade the observed intrinsic resolution of detectors. There are at least two sources of mechanical instabilities: (i) slight movements of setup elements in response to changes in ambient temperature or humidity; (ii) mechanical transients arising from slowly relaxing stresses in positioning stages, cabling, etc. The obvious way of improvement of the situation is to use stiffer mechanics. The other way is to use sliding alignment. The achievable improvement is given by sample size behavior of alignment precision and by the rate of mechanical misalignment. With the mechanical drift rate unchanged, the efficiency of re-alignment depends on the track acquisition rate; when track rate is small, the alignment has to be averaged over longer time intervals. A simplified re-alignment procedure was used in the beam test analysis: only shifts of detectors perpendicular to the beam (x and y) were updated. They were calculated as median residuals in residual plots (that is, plots of residuals vs. coordinate).

5.3. Correction of edge effect and other response distortions

Similarly to instabilities over time due to mechanical drifts, irregularities in the positional response of DEPFET sensors were observed as patterns of systematic bias in residual plots. Such

irregularities shift space points by tenths of microns to several microns. The correction simply subtracts median residuals (across a run) for each position from the residuals of individual track fits.

5.4. Sub-pixel analysis

The high resolution of the telescope system and available analysis methods allowed us to map variations of detector properties within a pixel. To calculate the response from a point within a pixel, a weighted average of 4000 closest tracks was calculated. The response was calculated on a grid of 9×18 points inside the area of the elementary cell (1×2 pixels) of the sensor matrix. Resolution maps are presented below.

5.5. Monte Carlo simulations

The verification of our analysis and validation of resolution estimates on simulated data serves as an important cross-check of the analysis methods and results. Simulations are even more "intrinsic" to the analysis—it is often the only or the most convenient way of estimating errors and sensitivity of analysis. The "full" simulations of particle tracks in the beam test setup were carried out using the ILC software framework [14]; the beam test setup (identical to that used in the analysis) was defined in the Mokka database and particle tracks were simulated by the GEANT4 engine. No digitization was used; instead, detector intrinsic resolutions were imitated by Gaussian smearing. A simple Marlin module was used to convert the LCIO data to ROOT trees. The simulated data underwent the same analysis as real data, starting from the track formation stage (cf. Section 4.1).

6. Results and discussion I: resolutions

Tracking residuals are key pre-requisites for the calculation of alignment (including corrections of mechanical movements), response distortion corrections, and resolutions. In this paper, "residuals" always mean "unbiased" residuals, i.e., residuals from track fits using hits in all other modules except the module in question.

6.1. Values

The values of residuals and intrinsic resolutions for two modules (DUT with pixel size $20 \times 20\ \mu m^2$ in position 2 and a reference plane with pixel size $32 \times 24\ \mu m^2$ in position 3) are shown in Table 1. The table also shows estimates of net tracking error (error of the telescope system in the limit of zero multiple scattering) and RMS contribution of multiple scattering to residual for 120 GeV pions. The reference planes at other positions of the setup were of the same type and have, within experimental error, the same intrinsic resolutions.

Table 1
Typical residuals and resolutions in x and y for 120 GeV pions. The systematic error is 0.1 μm. The values of residuals and resolutions are representative for several combinations of conditions and algorithms.

(μm)	Module 2 (DUT) $20 \times 20\ \mu m^2$		Module 3 (ref. plane) $32 \times 24\ \mu m^2$	
	x	y	x	y
Residual	1.54	1.42	1.98	1.61
Resolution	1.10	1.00	1.60	1.20
Net tracking error	0.73	0.62	0.86	0.73
Multiple scattering	0.76		0.79	

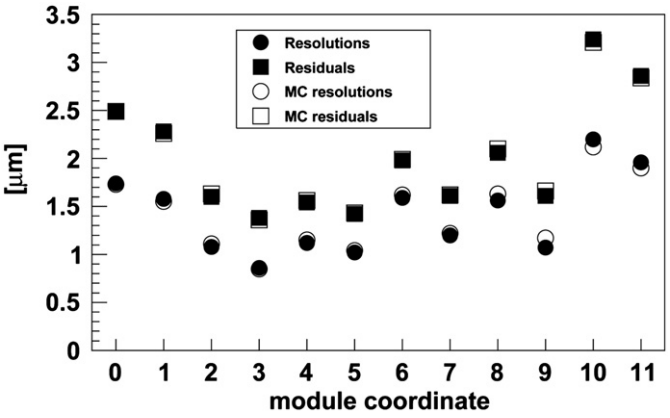

Fig. 6. Comparison of residuals (squares) and resolutions (circles) from the analysis of beam test data (solid) and simulated data (hollow) with representative resolutions set for all detector coordinates (0=plane 0, x; 1=plane 0, y; 2= plane 1, x, etc.).

6.2. Monte Carlo verification

Results of MC studies are shown in Fig. 6. The plot shows the resolutions extracted from the real and simulated data by the analysis. Apparently, in the low multiple scattering regime with the 120 GeV beam, the analysis reproduces the true values with satisfactory precision.

6.3. Factors influencing the intrinsic resolutions

Several factors can degrade the observed intrinsic resolutions. Fortunately, most distortions lead to worse (numerically larger) resolutions than the true ones,[2] so usually a decrease in observed resolutions means an improvement in analysis.

Gain correction: An uncertainty in pixel gains directly affects the position resolution: when calculating COG from two pixels, 1% error in gain leads to up to 0.5% error in position, equivalent to 0.5% of pitch—that is, tenths of microns, which is measurable. But to measure gains with 1% accuracy, distributions of 10^4 signals have to be equalized. For large pixel arrays, this means really huge statistics that may be pretty tricky to achieve.

In our beam test, the accumulated data allowed the calculation of pixel gains with about 4% precision, which was about the level of spread of actual pixel gains, so the application of the calculated pixel gains gave no visible improvement in resolutions.

Hit reconstruction: Centre-of-gravity (COG) position estimates for signal clusters were calculated from 2×2 pixels with the largest summary signal in a cluster. This gives best results for detectors with average cluster size less than 2 in every axis, or with full cluster size less than 4. For approximately perpendicular tracks of particles and modules with thickness of 450 μm, this condition is usually fulfilled for pixel sizes over $24 \times 24\ \mu m^2$. The DUT module has a smaller pixel size ($20 \times 20\ \mu m^2$) and its average cluster size exceeded 2×2. For this module, the best resolution was obtained for COG calculated from 3×3 pixels.

For position calculation, only pixels with signals over $2.6 \times$ average noise were accepted. For every direction, position and its error were calculated independently as signal- and noise-weighted means and standard deviations.

η corrections are applied as two independent one-dimensional η corrections in both coordinates. They are calculated in the traditional manner [10], with the exception that, in each direction, hit occupancy is equalized over two pixels rather than one.

[2] An important counter-example is biased sampling, such as tight cuts on fit χ^2.

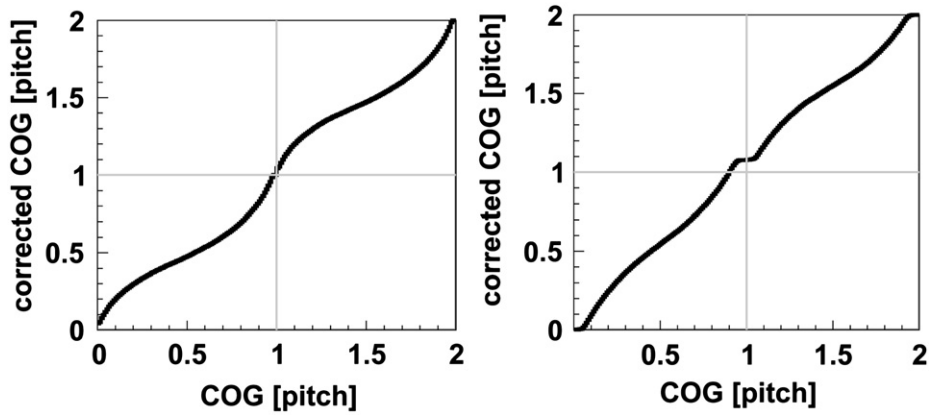

Fig. 7. Example of η correction functions in x (left) and y (right) directions.

This is due to the specific structure of the DEPFET sensor matrix, see Section 3.2. Examples of typical η correction functions are shown in Fig. 7. The asymmetry mentioned in Section 3.2 manifests clearly in these plots: in the y direction (right plot) there is, for every module, a visible shift upwards with respect to the symmetrical value expected in case of equal pixels.

The efficiency of "double-pixel" η correction compared to a "single-pixel" η is visible in intrinsic resolutions.

Mechanical stability: With longer acquisition times, mechanical instabilities of the detector setup become an issue. The solution is to re-calculate alignment regularly during the run. The frequency of re-alignment is given by the number of tracks needed to calculate a reasonably precise (correction of) alignment. This is about 1000 tracks for the DEPFET beam test setup. Thus, the limit of improvement are misalignment drifts occurring within the time needed to acquire 1000 particle tracks. This is about 4.5 min for 120 GeV pions, but 61 min for 40 GeV electrons. Therefore, the results for electrons are much more likely to be affected by slow variations in the setup.

An 8 h long run was used to test for the effect of mechanical instabilities. For the analysis, the run was split into sections of about 1000 tracks. Fig. 8 shows the distributions of median residuals in x and y directions before the alignment updates.

Correction of positional response distortions: The positional response distortion effects are in fact several different distortions that are treated by a common correction—"residual plot detrending": edge effects and other pixel-to-pixel differences uncorrected by gain correction.

The correction improves tracking and leads to narrower distributions of residuals, which indicates that the correction is effective.

An example of a residual plot before correction is in Fig. 9. The range of corrections is ± 20 μm for edge effects.

Factors influencing resolutions. Summary: Below we give estimates of the impact of individual analysis steps on RMS residuals and resolutions of DEPFET detectors in the settings of the beam test (specifically, 120 GeV pion beam, and the given typical distance between detectors):

1. Gain correction (internal property of DEPFET): no observed influence with given statistics.
2. COG estimates (internal properties of pixels, cluster size): variations between various estimators at the level of 0.03−0.3 μm.
3. η-correction (single/double pixel η): influence at the level of 0.03 μm in y.
4. Mechanical instability (running alignment on the timescale of tens of minutes): influence at the level of 1.0 μm.

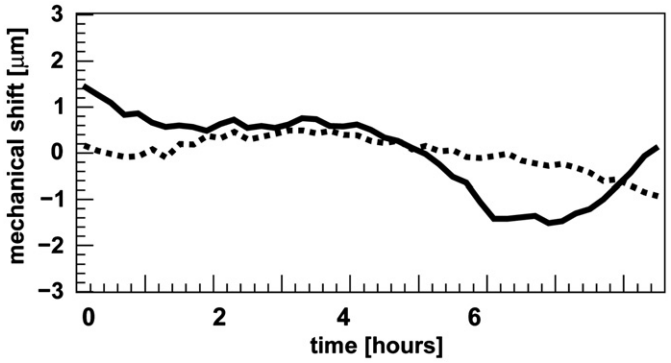

Fig. 8. Mechanical shifts of Module 2 during an 8 h run. The plots show median residuals before re-alignment vs. time. Solid—vertical, dotted—horizontal direction.

5. Response distortions correction or edge cut 0.25 mm from detector perimeter (internal property of DEPFET): average influence at the level of 0.2 μm.
6. Removal of one module from analysis (setup and analysis property), influence at the level of 0.1 μm (assessed as a systematic error of analysis algorithm), repeatability of analysis on similar data subsets is better than 0.01 μm.

7. Results and discussion II: studies using resolutions

In this section, three typical beam test studies are presented to illustrate the use of intrinsic resolutions.

7.1. Bias scan

For DEPFET sensors, the bias voltage is the voltage at the p^+ backside contact ("9" in Fig. 1). The bias scan was performed for voltages from 100 to 200 V. The plot of resolutions vs. bias voltage is shown in Fig. 10. The resolutions visibly stabilize above 160 V.

7.2. Angle scan

The angle scan was originally performed for a wide range of angles; here we only show the results for small tilts between $-6°$ and $4°$ around y axis on the DUT (module 2). The results were already published in Ref. [15] and are reproduced here as a typical beam test study.

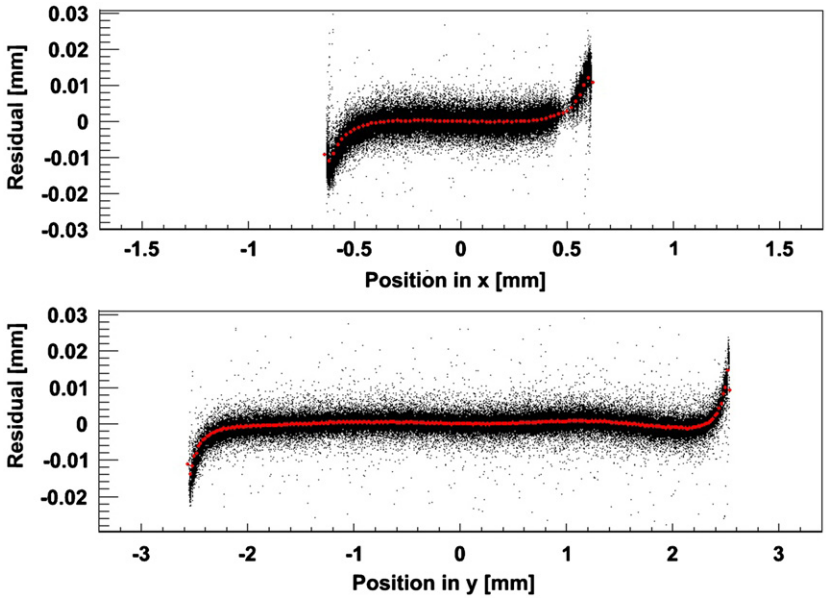

Fig. 9. Residuals vs. hit position; positional response distortions before correction. Edge effect is clearly visible in both coordinates. The correction (light gray line) is based on median residuals at a given position.

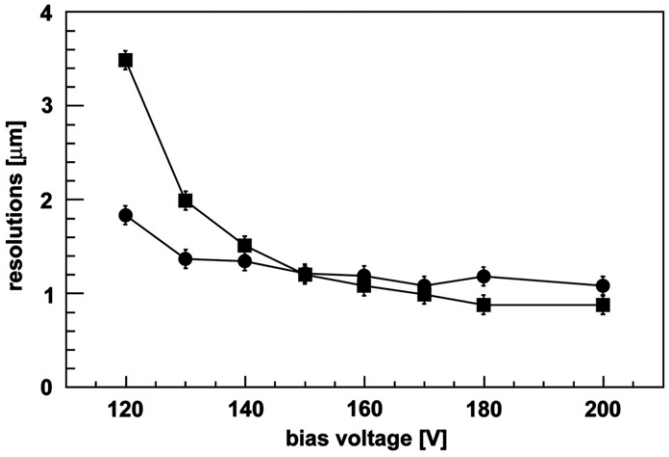

Fig. 10. Bias scan: resolutions in x (circles) and y (squares) for the detector with pixel size 20 × 20 μm.

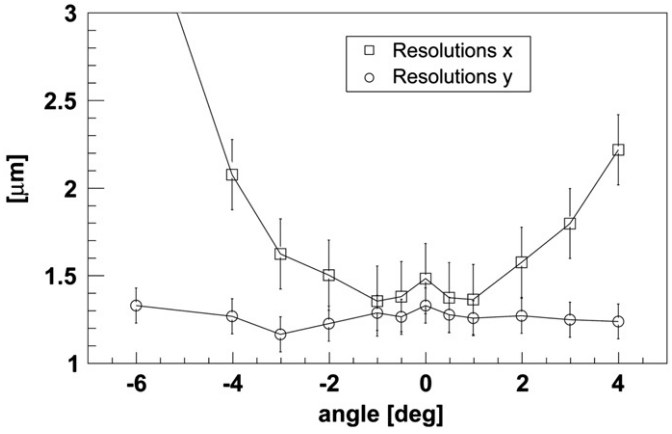

Fig. 11. Resolution vs. incidence angle for the DUT with pixel size 24 × 24 μm in direction x (squares) and y (circles).

The results are summarized in Fig. 11. The tilt of a module affects all calculated values in a predictable way. Residuals and resolutions are changed only in the x direction, that is, perpendicular to the tilt axis. Only in this direction the tilting increases the charge sharing and the cluster size. At small tilts the resolution improves as the charge sharing improves position reconstruction compared to zero tilt. At larger tilts, the resolution deteriorates as the increasing cluster size leads to a deterioration of the S/N ratio of pixel signals.

7.3. Energy scan

The energy scan was performed at the nominal beam energy of 120 GeV, with well-known particle and energy spectra, and at derivative energies of 100 and 80 GeV for pions, and 100, 80, 60 and 40 GeV for electrons. For all beam energies a good statistics for analysis has been acquired. However, the small acquisition rates at the lowest electron energies (61 and 33 min per 1000 tracks for 40 and 60 GeV electrons, respectively, vs. 4.5 min for 120 GeV pions) mean that mechanical instabilities cannot be

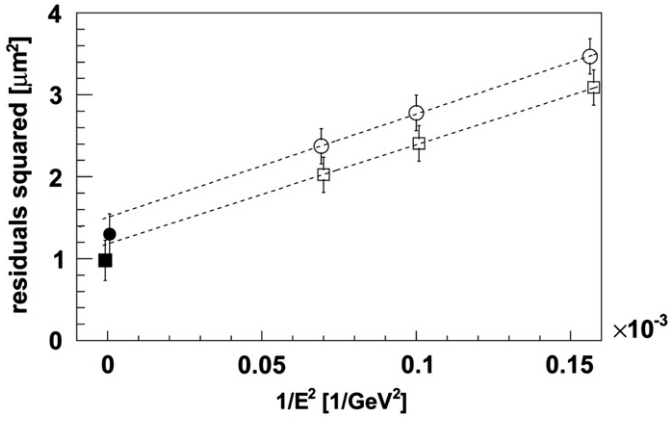

Fig. 12. Squared residuals vs. squared inverse energy with extrapolation to infinite energy for pions: x, hollow circles; y, hollow squares. The solid marks at infinite energy are the respective intrinsic resolutions calculated directly.

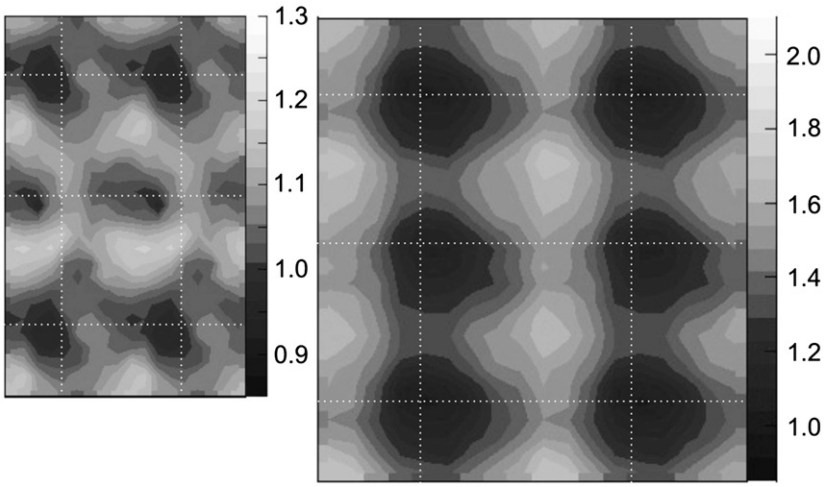

Fig. 13. Maps of resolutions in pixel area (see also Table 2) for detector 2 (left, 20 × 20 μm pitch) and detector 3 (right, 32 × 24 μm pitch). Map dimensions correspond to pitch, but the gray scales are different.

Table 2
Pixel-scale variation of residuals and resolutions.

	Module	Approximate range, x	Approximate range, y
Residuals in μm	20 × 20	1.4–1.6	1.2–1.5
	32 × 24	1.5–2.4	1.4–1.85
Resolutions in μm	20 × 20	1.0–1.2	0.8–1.2
	32 × 24	1.0–2.0	0.9–1.5

compensated as well as at higher energies. Moreover, the electron beam changed its position in space for different energies and the detector setup had to be re-aligned for each beam energy, which lead to mechanical transients from cabling and positioning stages. For these reasons, the results for electrons are not shown.

This scan is primarily a test of resolution estimates: the varying multiple scattering contribution must be properly unfolded from the measured residuals to give constant resolutions at all energies.

Fig. 12 shows infinite energy extrapolation for pions superposed with actual resolutions calculated for the detector. Apparently, the extrapolation is in a reasonably good agreement with the calculated resolutions.

8. Results and discussion III: pixel mapping

Detector response was mapped against hit position within a (double) pixel. Such an analysis was performed for central detectors of the beam test setup with 20 × 20 μm pitch and 32 × 24 μm pitch.

Maps of resolutions within a sensor cell for the two detectors are shown in Fig. 13. Table 2 lists approximate ranges of variation of residuals and resolutions over the double-pixel area. Due to its fine pitch, detector 2 is better in both directions as regards homogeneity of response.

Variation of resolution over the pixel area means that the definition of intrinsic resolution of a detector has to be slightly updated: it is the root-mean-square error of position measurement in a detector *averaged over pixel area*. The knowledge of pixel variations allows to improve hit reconstruction and tracking, which may be of interest in high-energy applications of the detectors.

9. Conclusions

This paper presents the results regarding intrinsic resolutions of the DEPFET pixel detectors based on data of DEPFET beam tests at CERN SPS.

Properties of the DEPFET pixel detectors were introduced and a description of beam test data analysis was given.

The paper is focused on detector intrinsic resolutions. Calculation of the resolutions is explained and several factors influencing the resolutions are discussed in more detail. Of these, a particular attention is given to mechanical instabilities, which are unavoidable due to long measurement times and seriously complicate beam energy scans.

The influence of other factors affecting intrinsic resolutions can be excluded or limited by proper working settings for detectors and by cautious analysis.

The presentations of the bias scan, angle scan and energy scan show that intrinsic resolution estimates behave regularly and are a reliable tool in detector studies.

Also, it is shown that intrinsic resolutions can be mapped on sub-pixel scales, and indeed vary on the scale of a pixel. Resolution mapping can help in providing more precise space points and errors for tracking in real high-energy physics experiments.

Acknowledgments

The authors acknowledge the support by BNBF Contract 05H09VH8 (University of Heidelberg and Bonn University), Volkswagen Foundation (Ariane Frey and Benjamin Schwenker), the Spanish Ministry of Education and Science Project FPA2008-05979-C04-03 (University of Santiago de Compostela), the Czech Science Foundation Grant no. 203/10/0777 and the Ministry of Education, Youth and Sports of the Czech Republic Contracts nos. LA10033 and MSM0021620859 (Charles University), and by EU FP6 (EUDET), Contract RII3-CT-2006-026126 (Stefan Rummel).

References

[1] DEPFET web: 〈http://www.depfet.org〉.
[2] J. Kemmer, G. Lutz, Nucl. Instr. and Meth. A 253 (1987) 356.
[3] J.J. Velthuis, et al., Nucl. Instr. and Meth. A 579 (2007) 685.
[4] G. Lutz, et al., Nucl. Instr. and Meth. A 572 (2007) 311.
[5] J.J. Velthuis, et al., IEEE Trans. Nucl. Sci. NS-55 (2008) 662.
[6] P. Kodys, et al., Nucl. Instr. and Meth. A 604 (2009) 385.

[7] D. Cussans, Description of the JRA1 Trigger Logic Unit (TLU), v0.2c, EUDET-Memo-2009-4, ⟨http://www.eudet.org⟩, September 2009.
[8] R. Kohrs, Development and characterization of a DEPFET prototype system for the ILC vertex detector, Ph.D. Thesis, Bonn University, 2008.
[9] G. Scott, H. Longuet-Higgins, Proc. R. Soc. London B244 (1991) 21.
[10] R. Turchetta, Nucl. Instr. and Meth. A 335 (1993) 44.
[11] ILC software/EUTelescope homepage: ⟨http://ilcsoft.desy.de/portal/software_packages/eutelescope/⟩.
[12] J. Furletova, L. Reuen, JRA1—the DEPFET sensor as the first fully integrated DUT in the EUDET pixel telescope: the SPS test beam 2008, EUDET-Memo-2008-34, ⟨http://www.eudet.org⟩, December 2008.
[13] R. Brun, F. Rademakers, Nucl. Instr. and Meth. A 389 (1997) 81 See also ⟨http://root.cern.ch/⟩.
[14] ILC software homepage: ⟨http://ilcsoft.desy.de⟩.
[15] P. Kvasnička, Nucl. Instr. and Meth. A., in press, doi:10.1016/j.nima.2010.06.170.
[16] W.-M. Yao, et al., J. Phys. G 33 (2006) 15 Available on the PDG WWW pages ⟨http://pdg.lbl.gov/⟩.